Available online at www.sciencedirect.com
ScienceDirect
Applied Catalysis B: Environmental 82 (2008) 120–130
APPLIED CATALYSIS B: ENVIRONMENTAL
www.elsevier.com/locate/apcatb

Biodiesel synthesis using calcined layered double hydroxide catalysts

J. Link Shumaker [a], Czarena Crofcheck [a,*], S. Adam Tackett [b], Eduardo Santillan-Jimenez [b], Tonya Morgan [b], Yaying Ji [b], Mark Crocker [b,**], Todd J. Toops [c]

[a] *Biosystems and Agricultural Engineering, University of Kentucky, 128 CE Barnhart Building, Lexington, KY 40546-0276, USA*
[b] *Center for Applied Energy Research, University of Kentucky, 2540 Research Park Drive, Lexington, KY 40511-8479, USA*
[c] *Fuels, Engines and Emissions Research Center, Oak Ridge National Laboratory, 2360 Cherahala Boulevard, Knoxville, TN 37932-1563, USA*

Received 6 July 2007; received in revised form 9 January 2008; accepted 15 January 2008
Available online 20 January 2008

Abstract

The catalytic properties of calcined Li–Al, Mg–Al and Mg–Fe layered double hydroxides (LDHs) were examined in two transesterification reactions, namely, the reaction of glyceryl tributyrate with methanol and the reaction of soybean oil with methanol. While the Li–Al catalysts showed high activity in these reactions at the reflux temperature of methanol, the Mg–Fe and Mg–Al catalysts exhibited much lower methyl ester yields. CO_2 TPD measurements revealed the presence of sites of weak, medium and strong basicity on both Mg–Al and Li–Al catalysts, the latter showing higher concentrations of medium and strong base sites; by implication, these are the main sites active in transesterification catalyzed by calcined Li–Al LDHs. Maximum activity was observed for the Li–Al catalysts when a calcination temperature of 450–500 °C was applied, corresponding to decomposition of the layered double hydroxide to the mixed oxide without formation of crystalline lithium aluminate phases.

Keywords: Transesterification; Triglyceride; Layered double hydroxide; Lithium; Aluminum

1. Introduction

The production of biodiesel from vegetable oil represents a well-established means of producing liquid fuels from biomass, and one which is rapidly growing in importance. Commercially, biodiesel is produced from vegetable oils such as soybean, rapeseed and sunflower oil, as well as animal fats. These oils and fats are typically composed of C_{14}–C_{20} fatty acid triglycerides, constituting ~90–95 wt.% of the oil. In order to produce a fuel that is suitable for use in diesel engines, the triglycerides are converted to the respective fatty acid esters (with glycerol as a co-product) by base-catalyzed transesterification with short chain alcohols (generally methanol) [1]. Transesterification is also an important reaction in the chemical industry, as exemplified by large-scale applications such as the production of polyethylene terephthalate (PET) [2]. Smaller scale applications include the synthesis of fatty acid monoesters of glycerol (monoglycerides) which are used in pharmaceuticals, cosmetics and as emulsifiers in food [3]. Monoglycerides can be obtained either via direct esterification of glycerol with fatty acids, or via the transesterification of glycerol with triglycerides or fatty acid esters.

Transesterification can be catalyzed by both acids and bases. Industrially, homogeneous base catalysts are used, including sodium or potassium hydroxides or alkoxides [1]. Base catalysis is preferred to the use of acid catalysts such as sulfuric or sulfonic acids, given the corrosivity and lower activity of the latter. However, removal of the base after reaction is problematic, since the current practice of aqueous quenching with acid results in some degree of saponification (i.e., hydrolysis of the ester and formation of the corresponding sodium carboxylate), as well as the formation of emulsions which render separation of the ester difficult. Further, an alkaline wastewater stream is generated. In order to circumvent these problems, the use of heterogeneous catalysts is of interest. In principle, this approach eliminates the need for an aqueous quench and largely eliminates the formation of metal salts, thereby simplifying downstream separation steps. Consequently, production costs should be reduced, albeit that the cost of the triglyceride starting material represents the majority of the total production cost [4]. Furthermore, the process should be rendered more environmentally friendly.

* Corresponding author. Tel.: +1 859 257 3000; fax: +1 859 257 5671.
** Corresponding author. Tel.: +1 859 257 0295; fax: +1 859 257 0302.
E-mail addresses: crofcheck@uky.edu (C. Crofcheck), crocker@caer.uky.edu (M. Crocker).

0926-3373/$ – see front matter
doi:10.1016/j.apcatb.2008.01.010

A wide variety of solid bases have been examined for this purpose. Examples include alkaline earth oxides [5–9], K- and Li-promoted oxides [10–13], calcined hydrotalcites [14,15], zeolites [7], anion exchange resins [5] and polymer-supported guanidines [16]. In addition, a continuous process for biodiesel production has been developed by IFP based on a heterogeneous zinc aluminate ($ZnAl_2O_4$) catalyst [17,18]. Although the activity of this catalyst is relatively low, necessitating the use of high reaction temperatures (~200 °C), it is reported to show very stable operation with no metal leaching (i.e., no formation of metal glycerate or carboxylate salts). The purity of the methyl esters produced is claimed to exceed 99%, with yields close to 100% of theoretical.

Recently Corma et al. [19] reported that calcined Li–Al and Mg–Al layered double hydroxides (LDHs) are able to catalyze the glycerolysis of fatty acid methyl esters to monoglycerides (the reverse of biodiesel synthesis). An uncalcined Li–Al LDH, $[Al_2Li(OH)_6]OH{\cdot}nH_2O$, has also recently been reported to be active in the transesterification of 5-carboxyfluorescein diacetate with 1-butanol [20]. In the former study [19], the Li–Al catalyst, corresponding to calcined $[Al_2Li(OH)_6](CO_3)_{0.5}{\cdot}nH_2O$, was reported to be more active than the Mg–Al material (or MgO) due to its higher Lewis basicity. This result prompted us to study the catalytic properties of calcined $[Al_2Li(OH)_6](CO_3)_{0.5}{\cdot}nH_2O$ in the synthesis of biodiesel from soybean oil [21]. At the reflux temperature of methanol, near quantitative conversion of the soybean oil was achieved at low catalyst loadings (2–3 wt.%) and short reaction times (~2 h). Recycling studies showed that the catalyst maintained a high level of activity over several cycles, although analyses indicated that a small amount of lithium was leached from the catalyst. In this paper we report an extension of these studies. In addition to soybean oil methanolysis, a model transesterification reaction has been studied, namely the reaction of glyceryl tributyrate with methanol. The effect of the preparation method on catalyst properties has been examined and experiments performed with calcined Mg–Al and Mg–Fe layered double hydroxides for comparison.

2. Experimental

2.1. Catalyst preparation

Mg–Al and Mg–Fe layered double hydroxides were prepared according to the method of Reichle [22]. A solution of $Mg(NO_3)_2{\cdot}6H_2O$ and either $Al(NO_3)_3{\cdot}9H_2O$ or $Fe(NO_3)_3{\cdot}9H_2O$ (0.4 mol total metals) in 210 ml deionized water was added dropwise at room temperature to 330 ml of an aqueous solution containing Na_2CO_3 (30 g, 0.28 mol) and the calculated amount of NaOH required to react with the M^{2+} and M^{3+} ions. Vigorous stirring was maintained throughout the ~60 min addition period. The resulting precipitate was left to age in the reaction mixture under gentle stirring at 75 °C overnight and was subsequently isolated by a cycle of centrifuging/decanting/washing with deionized water until the washings attained a pH of 7. The resulting solid was dried at 60 °C in a vacuum oven. The measured residual sodium content was in all cases <500 ppm. To produce mixed oxides, the LDHs were calcined in air at 450 °C for 2 h. The resulting mixed oxides were stored in a vacuum dessicator. High surface area MgO was prepared by a standard precipitation method [23].

$[Al_2Li(OH)_6](CO_3)_{0.5}{\cdot}nH_2O$ was prepared according to three different literature procedures [24–26]:

- *LiAl-1*. An aqueous solution of $Al(NO_3)_3{\cdot}9H_2O$ (250 ml, 0.4 M) was added dropwise at room temperature to 600 ml of a mixture of $LiOH{\cdot}H_2O$ (1.5 M) and Na_2CO_3 (0.08 M) in deionized water. Vigorous stirring was maintained throughout the ~60 min addition period. The resulting precipitate was left to age in the reaction mixture under gentle stirring at 75 °C overnight and isolated as described above. The residual Na content (by inductively coupled plasma-optical emission spectroscopy, ICP-OES) was 162 ppm.
- *LiAl-2*. A solution of $Al(O^sBu)_3$ in toluene (200 ml, 0.61 M) was added dropwise at room temperature to an aqueous solution of Li_2CO_3 in deionized water (450 ml, 0.14 M). Vigorous stirring was maintained throughout ~60 min addition period. The resulting precipitate was allowed to age and isolated as described above.
- *LiAl-3*. An aqueous solution of $Al_2(CO_3)_3$ (400 ml, 0.5 M) was added dropwise at room temperature to an aqueous solution of $LiOH{\cdot}H_2O$ (50 ml, 4.8 M). The addition was continued until the mixture attained a pH of 10. Vigorous stirring was maintained throughout the addition period. The resulting precipitate was allowed to age and isolated as described above.

2.2. Catalyst characterization

Surface area and pore volume measurements were performed according to the BET method by nitrogen adsorption at −196 °C using a Micromeritics Tri-Star system. Catalyst samples were outgassed overnight at 160 °C under vacuum prior to the measurements. The chemical composition of the catalysts was determined using ICP-OES. Powder X-ray diffraction (XRD) measurements were performed on a Phillips X'Pert diffractomer using Cu Kα radiation (λ = 1.5406 Å) and a step size of 0.02°. Peak simulation was performed using a standard fitting program [27]. Average crystallite sizes were calculated using Fourier integral breadth analysis. Scanning electron microscopy (SEM) was performed using a Hitachi S-2700 instrument equipped with a LaB_6 electron gun and a PGT EDS analyzer with thin window detector. XPS analyses were performed on a PHI 5600 LS instrument, using a non-monochromatic Al source. The analysis area was 1 mm × 3 mm. The C 1s line (285.0 eV) was employed as a binding energy standard.

Hammett indicator experiments were conducted to determine the H_- range of basic sites in each catalyst [28]. The Hammett indicators used were neutral red ($pK_a = 6.8$), phenolphthalein ($pK_a = \sim 9.3$), Nile blue ($pK_a = 10.1$), alizarin yellow R ($pK_a = 11.0$), indigo carmine ($pK_a = 12.2$) and 2,4-dinitroaniline ($pK_a = 15$). Although Hammett indicator measurements are usually performed in non-polar solvents, anhydrous methanol was used in this case in order to provide a more realistic assessment of base strength under transesterification conditions.

Typically, 25 mg of catalyst was mixed with 4 ml of indicator solution, shaken, and allowed to sit for at least 1 h. The basic strength of the catalyst was taken to be higher than the weakest indicator that underwent a color change and lower than the strongest indicator that underwent no color change.

CO_2 temperature programmed desorption (TPD) experiments were performed using a microreactor loaded with 100 mg of sample. The LDH was first calcined *ex situ* for 2 h at 450 °C. A weighed amount of freshly calcined material was then placed in the reactor and further treated for 30 min at 450 °C under Ar. The sample was then cooled to 80 °C prior to adsorption of CO_2 (1% in Ar, 100 sccm for 1 h). The system was flushed with Ar for 30 min at 80 °C, after which the temperature was ramped to 500 °C (10 °C/min) and held at this temperature for 15 min. Effluent gases were analyzed using a mass spectrometer (SRS RGA100).

2.3. Transesterification of glyceryl tributyrate

The method of Cantrell et al. [15] was used for the transesterification of glyceryl tributyrate. Reactions were performed at reflux temperature (65 °C) in a stirred batch reactor using glyceryl tributyrate (Aldrich, 98%, 6 ml, 20 mmol), dihexyl ether (0.950 g, 5.0 mmol) as internal standard, anhydrous MeOH (25 ml, 600 mmol) and 0.1 g catalyst. To avoid diffusional limitations, catalysts were tested as fine powders (ca. 200 mesh) and reaction mixtures were stirred at the maximum rate achievable (~850 rpm). Duplicate tests performed at half this stirring rate yielded reaction rates that were almost unchanged, indicating that mass transport effects were minimal. Samples were withdrawn for analysis at reaction times corresponding to 0 min, 5 min, 10 min, 15 min, 25 min, 40 min, 60 min, 120 min and 180 min. Samples were quenched on ice for 2 min, and then filtered and analyzed using a Hewlett-Packard 5890 Series II gas chromatograph equipped with a HP-5 cross-linked 5% phenylmethylsiloxane column (30 m length, 0.32 mm internal diameter, 0.25 μm film thickness).

2.4. Transesterification of soybean oil

Fifteen grams of soybean oil (Spectrum Naturals, expeller pressed organic soy oil, acid value of <0.1 mg KOH/g, 0.02% water by Karl Fisher titration) was weighed into a 100 ml two-neck flask, to which anhydrous methanol (Aldrich, <0.002% water, 10.4 ml, equivalent to a MeOH:oil mole ratio of 15) was added. The mixture was stirred vigorously and heated to reflux temperature, whereupon the appropriate amount of catalyst (1–3 wt.% relative to vegetable oil) was added. The reaction was allowed to proceed for a specified amount of time (1–6 h), after which the mixture was filtered to remove the catalyst. Methanol was removed from the filtrate on a rotary evaporator, after which the product was washed with saturated aqueous sodium chloride (3 × 50 ml) and dried over sodium sulfate. Oil conversions were determined using the ^{1}H NMR technique described by Gelbard et al. [29] on a Varian Gemini-200 instrument operating at 200 MHz. As reported in [29], the methylene protons adjacent to the ester groups in the triglyceride and fatty acid methyl esters appear at 2.3 ppm and the methoxy protons of the methyl esters appear at 3.7 ppm. By integrating the areas (A) under the signals at 2.3 ppm and 3.7 ppm and using the following equation, the yield of methyl esters was calculated:

$$\text{methyl esters yield } (\%) = 100 \times \left(\frac{2A_{3.7}}{3A_{2.3}}\right)$$

Note that this yield is equivalent to the conversion of triglyceride to methyl esters (i.e., product of triglyceride conversion and selectivity to methyl esters). Mono- and diglyceride yields are not determined by this method.

Used catalyst from the above runs was washed with successively methanol, toluene and pentane and dried overnight in a vacuum oven at 100 °C. The resulting samples were analyzed for Li and Al by ICP-OES and XPS.

3. Results and discussion

3.1. Physical characterization of catalysts

For the preparation of $[LiAl_2(OH)_6](CO_3)_{0.5}{\cdot}nH_2O$, three different literature procedures were examined. According to elemental analysis (Table 1), in each case the Al:Li stoichiometry in the product is close to the expected value of 2. In our previous work [21], $[LiAl_2(OH)_6](CO_3)_{0.5}{\cdot}nH_2O$

Table 1
Elemental analysis and XPS data for Li–Al catalysts

Sample	ICP-OES			XPS				
	Li (wt.%)	Al (wt.%)	Al/Li	Li (at.%)	Al (at.%)	Al/Li	O (at.%)	C (at.%)
LiAl-1	3.2	24.0	1.9	3.0	12.4	4.1	65.4	19.2
Calcined LiAl-1	5.1	42.6	2.2	10.6	26.8	2.5	55.4	7.1
Spent calcined LiAl-1[a]	4.1	37.0	2.3	5.9	19.7	3.3	60.3	13.4
LiAl-2	3.2	27.9	2.2	2.7	13.6	5.0	66.6	15.8
Calcined LiAl-2	–	–	–	12.8	26.4	2.1	53.3	7.4
Spent calcined LiAl-2[a]	4.3	39.2	2.3	6.7	20.0	3.0	59.7	13.6
LiAl-3	2.9	23.3	2.1	2.8	13.7	4.9	69.4	13.0
Calcined LiAl-3	5.1	41.8	2.1	13.6	27.2	2.0	51.6	7.6
Spent calcined LiAl-3[a]	4.0	35.9	2.3	5.2	20.5	3.9	60.7	13.6

[a] Spent catalyst from experiment summarized in Table 7.

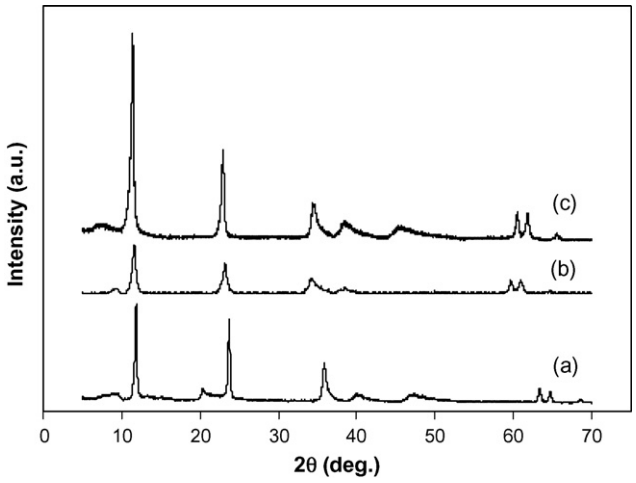

Fig. 1. Powder X-ray diffractograms of selected layered double hydroxides: (a) LiAl-1; (b) $Mg_{0.69}Fe_{0.31}$; (c) $Mg_{0.73}Al_{0.27}$.

prepared by addition of aqueous $Al(NO_3)_3{\cdot}9H_2O$ to a mixture of $LiOH{\cdot}H_2O$ and Na_2CO_3 was obtained with an Al/Li stoichiometry of 4.3. However, upon repetition of this synthesis method, as for the preparation of sample LiAl-1 (Table 1), we find that the expected stoichiometry is obtained. XPS data confirmed the presence of Li in the samples, although in each case the measured atomic Al:Li ratio determined by XPS is higher than the ratio determined by ICP-OES, suggesting a surface enrichment of aluminum. Diffractograms (Fig. 1) were consistent with the presence of crystalline $[LiAl_2(OH)_6](-CO_3)_{0.5}{\cdot}nH_2O$, the observed *d*-spacings being in agreement with published values [25].

Measured BET surface areas of the materials (Table 2) were found to span a fairly narrow range, that of LiAl-3 (96 m^2/g) being slightly higher than those of LiAl-1 (78 m^2/g) and LiAl-2 (72 m^2/g). Upon calcination at 450 °C the Li–Al LDHs decomposed via decarboxylation and dehydroxylation [21], corresponding to a loss in sample mass of ca. 45%. Simultaneously the surface areas and the pore volumes of the samples increased significantly, although there was no apparent correlation between the surface area of the LDH and the final surface area of the calcined material. This increase in surface area upon LDH calcination has been attributed to the formation of micro- and mesopores due to expulsion of CO_2 and H_2O from the LDH [30,31]. The loss of CO_2 and H_2O is

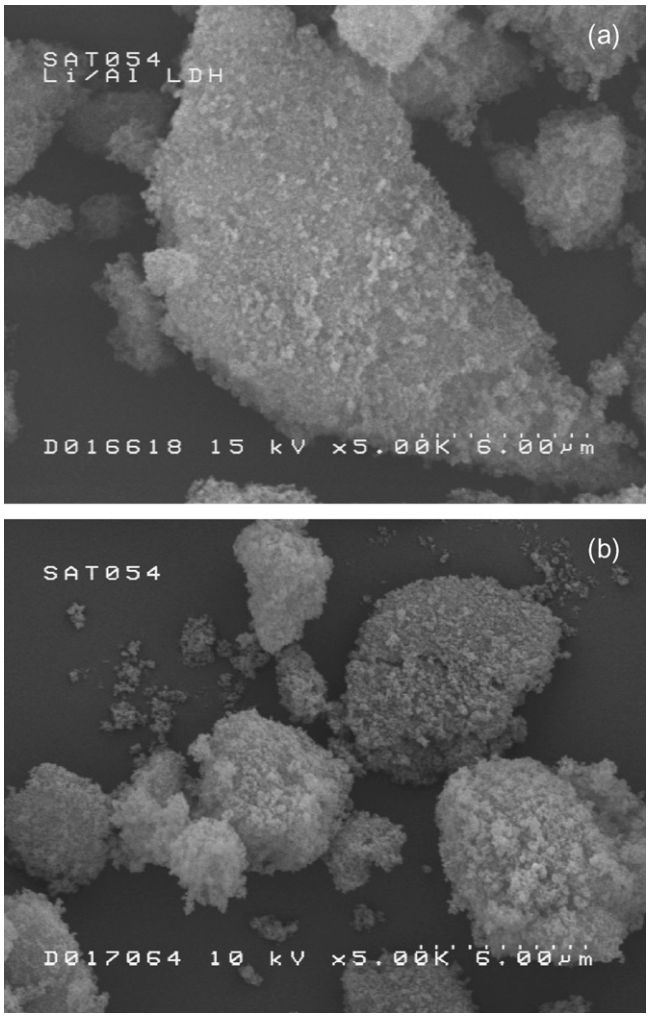

Fig. 2. Scanning electron micrographs of (a) LiAl-1 (as synthesized) and (b) LiAl-1 after calcination at 450 °C for 2 h.

also reflected in increased Al and Li concentrations in the calcined samples, relative to the uncalcined analogs, as shown by the results of ICP-OES and XPS measurements (see Table 1). Diffractograms of the materials calcined at 450 °C (not shown) revealed them to be largely amorphous, although very broad, weak diffraction lines were observed at ca. $2\theta = 37^\circ$ and 65° which can be attributed to poorly crystalline γ-Al_2O_3.

Scanning electron micrographs of the Li–Al LDHs reveal that the preparation route has a significant influence on the

Table 2
Physical data for as-prepared LDHs and the mixed oxides derived from them[a]

Catalyst	LDH surface area ($m^2\ g^{-1}$)	LDH pore volume ($cm^3\ g^{-1}$)	Mean LDH crystallite size (Å)[b]	Mixed oxide surface area ($m^2\ g^{-1}$)	Mixed oxide pore volume ($cm^3\ g^{-1}$)
LiAl-1	78	0.293	256	293	0.455
LiAl-2	72	0.312	196	221	0.516
LiAl-3	96	0.545	113	227	0.653
$Mg_{0.73}Al_{0.27}$	80	0.483	169	209	0.636
$Mg_{0.66}Al_{0.34}$	139	0.847	60	242	1.185
$Mg_{0.69}Fe_{0.31}$	140	0.438	144	213	0.58
MgO	–	–	–	205	0.399

[a] Mixed oxides prepared by LDH calcination at 450 °C for 2 h.
[b] Measured in 0 0 *l* direction.

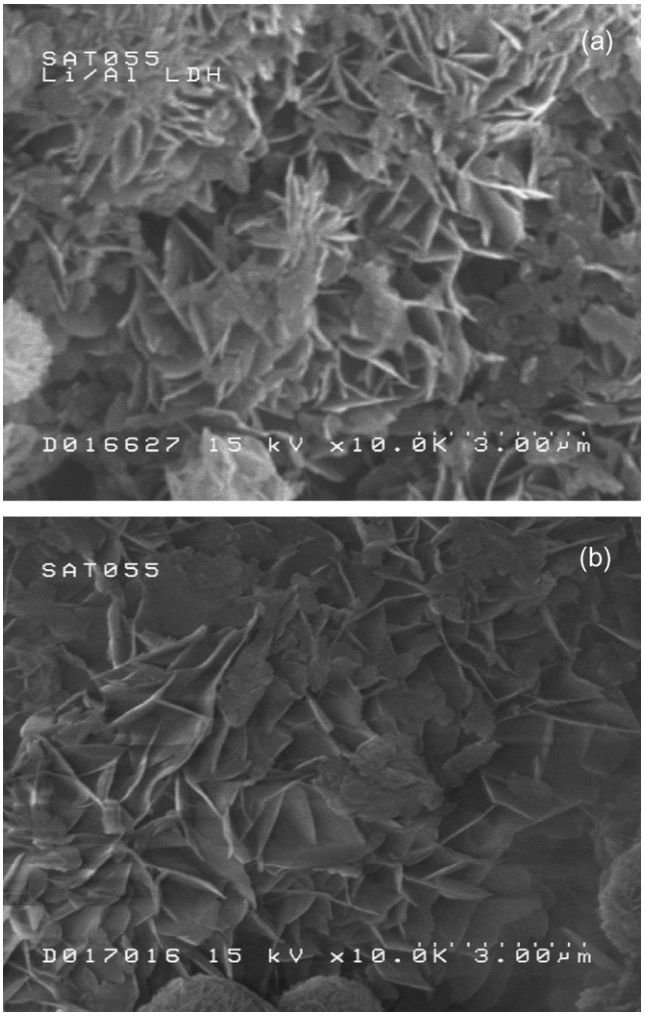

Fig. 3. Scanning electron micrographs of (a) LiAl-3 (as synthesized) and (b) LiAl-3 after calcination at 450 °C for 2 h.

morphology of the LDH. As shown in Fig. 2(a), as-synthesized LiAl-1 consists of compact agglomerates of non-porous grains, which are poorly crystalline. Near identical micrographs were obtained for LiAl-2 (not shown). A similar morphology has been noted previously for $[LiAl_2(OH)_6](CO_3)_{0.5}{\cdot}nH_2O$ prepared according to the same precipitation method as LiAl-2 [26], and for LDHs of the type $[LiFe_xAl_{2-x}(OH)_6](CO_3)_{0.5}{\cdot}nH_2O$ [32]. In contrast, micrographs of LiAl-3 (Fig. 3(a)) reveal the presence of platelets, many of which are hexagonal in form; this morphology is typical of well-crystallized hydrotalcite-type compounds. The fact that the platelets pack to form a rather open network helps to explain the higher porosity of LiAl-3 as compared to the more densely packed structures in LiAl-1 and -2.

Nitrogen adsorption/desorption isotherms for LiAl-1 and LiAl-3 are shown in Fig. 4. Both samples exhibit type IV isotherms characteristic of mesoporous materials [33]. The hysteresis loop is small and possesses features reminiscent of both the H3 and H1 type (IUPAC classification). The fact that adsorption appears to be limiting at high P/P_0 suggests that the latter classification is a more valid description. Type H1 hysteresis is usually associated with solids consisting of nearly cylindrical channels or agglomerates or compacts of near uniform spheres. In each case, the hysteresis loop is narrow, with almost parallel adsorption and desorption branches. This is indicative of pores with regular geometry, while the steep desorption behavior indicates that the dimensions of the pores fall in a narrow range. This is clearly seen in the corresponding pore size distribution plots (Fig. 5), which show a very narrow distribution for LiAl-1 centered at ca. 35 nm pore radius. For LiAl-3 the distribution is broader, the measured pore radii extending down to below 10 nm.

Micrographs of LiAl-1 and LiAl-3 calcined at 450 °C are shown in Figs. 2(b) and 3(b), respectively. From these it is apparent that the gross structural features of the compounds are retained, indicating that decomposition of the LDHs proceeds

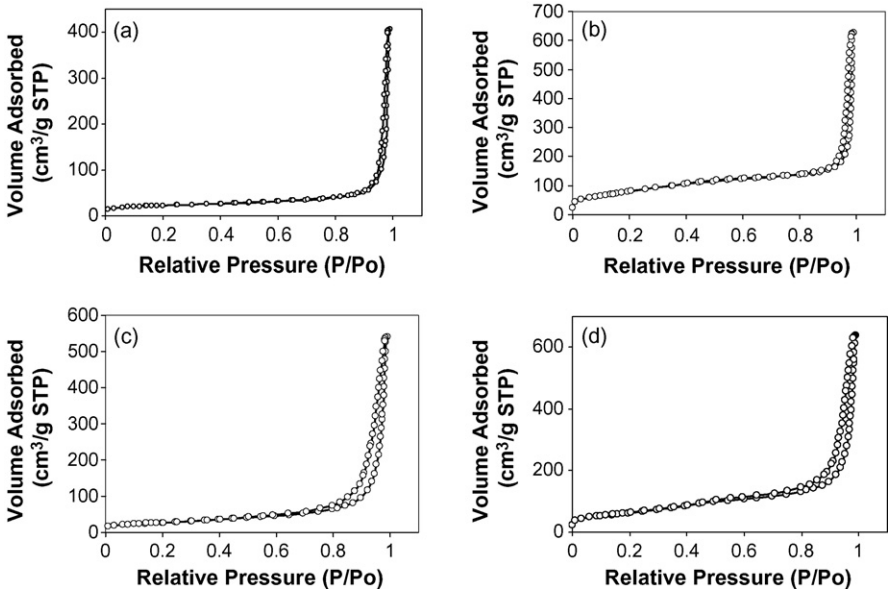

Fig. 4. N_2 adsorption/desorption isotherms for (a) LiAl-1 (as synthesized); (b) LiAl-1 after calcination at 450 °C; (c) LiAl-3 (as synthesized); (d) LiAl-3 after calcination at 450 °C.

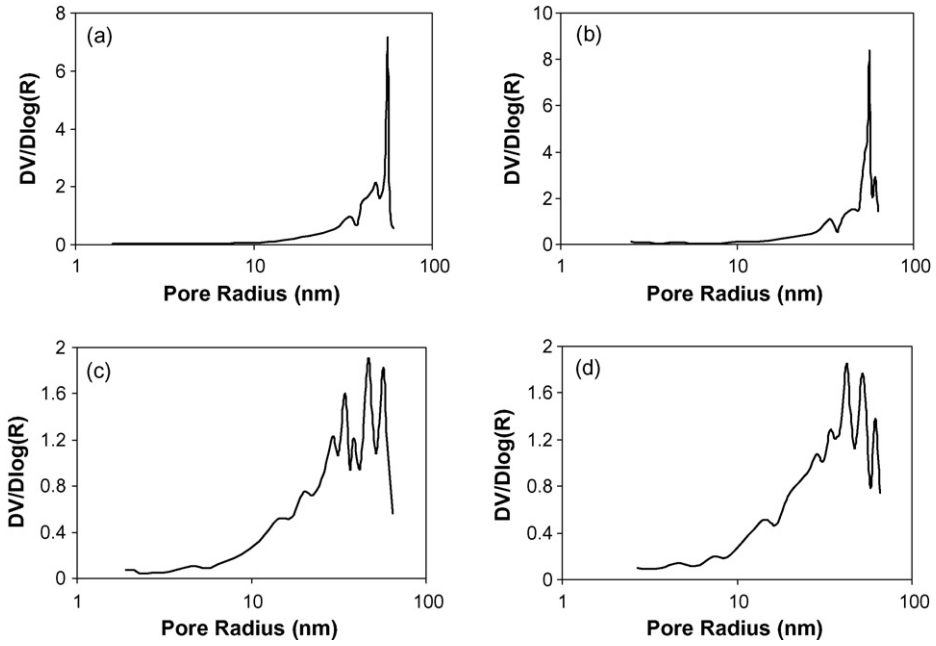

Fig. 5. Pore-size distribution plots derived from N_2 adsorption isotherms for (a) LiAl-1 (as synthesized); (b) LiAl-1 after calcination at 450 °C; (c) LiAl-3 (as synthesized); (d) LiAl-3 after calcination at 450 °C.

topotactically, as observed for Mg–Al and Ni–Al LDHs [34]. In the case of LiAl-3, collapse of the lamellar structure is evidenced by the presence of deformations in many of the platelets in the 0 0 *l* plane. Although both samples exhibit increased surface area and pore volume after calcination, the shapes of the nitrogen isotherms do not change significantly. Similarly, the pore size distributions are little changed in the mesoporous region. *t*-Plots revealed an absence of micropores in the calcined materials, indicating that exclusively mesopores were created during the thermal expulsion of CO_2 and H_2O.

For comparison purposes, a number of magnesium-containing LDHs were prepared. These included two Mg–Al LDHs, with nominal Mg/Mg + Al ratios of 0.75 and 0.67. Elemental analysis (Table 3) indicated good agreement between the measured and nominal compositions, i.e., the measured metal ion ratios (Mg/Mg + Al = 0.73 and 0.66, respectively) were the same as those used in the synthesis solution (within analytical error). Additionally an LDH containing Mg and Fe was prepared, in order to study the effect of replacing Al with Fe on LDH surface area and basicity. The Mg–Al and Mg–Fe LDHs in all cases exhibited X-ray diffractograms characteristic of hydrotalcite-type compounds (Fig. 1) [22], albeit that the Mg–Fe material was less crystalline. Calcination resulted in decomposition of the LDHs into the corresponding mixed oxides with increased surface area and pore volume. From Table 2 it is apparent that replacing Al with Fe had little effect on the textural properties of the initial LDH, or its calcined form.

The strength of the basic sites in the calcined LDHs was analyzed qualitatively using Hammett indicators. As shown in Table 4, the three Li–Al samples were found to possess H_- values in the range 11–12.2, while the Mg–Al and Mg–Fe samples were more basic, as evidenced by their ability to effect a color change with indigo carmine ($pK_a = 12.2$). Slightly different results have been reported by Kagunya et al. [35], calcined Mg–Al and Li–Al LDHs in their study being found to possess similar basicity according to Hammett indicator measurements. This may reflect the different calcination conditions used in their study (450 °C, 14 h), or the fact that a different solvent was used for the measurements (benzene or dichloromethane instead of methanol).

CO_2 TPD measurements were also performed for the assessment of basic site strength and concentration. Fig. 6 shows the rate of CO_2 desorption, normalized to the sample loading, as a function of the run time and temperature for calcined LiAl-3 and $Mg_{0.73}Al_{0.27}$. The desorption profiles are qualitatively similar, and can be deconvoluted into three desorption bands showing maxima at 144, 228 and 500 °C. The

Table 3
Elemental analysis data for Mg–Al and Mg–Fe LDHs and XPS data for the mixed oxides derived from them

Sample	Layered double hydroxide: ICP-OES			Mixed oxide: XPS		
	Mg (wt.%)	Al (wt.%)	Fe (wt.%)	Mg (at.%)	Al (at.%)	Fe (at.%)
$Mg_{0.73}Al_{0.27}$	20.5	8.3	–	26.1	12.0	–
$Mg_{0.66}Al_{0.34}$	18.0	10.4	–	24.9	7.6	–
$Mg_{0.69}Fe_{0.31}$	17	–	17.8	18.6	–	3.9
MgO	–	–	–	40.3	–	–

Table 4
Results of Hammett indicator measurements on calcined layered double hydroxides[a]

Catalyst	Base strength
LiAl-1	$11 < H_- < 12.2$
LiAl-2	$11 < H_- < 12.2$
LiAl-3	$11 < H_- < 12.2$
$Mg_{0.66}Al_{0.34}$	$12.2 < H_- < 15$
$Mg_{0.73}Al_{0.27}$	$12.2 < H_- < 15$
$Mg_{0.69}Fe_{0.31}$	$12.2 < H_- < 15$

[a] Calcination at 450 °C for 2 h.

amount of evolved CO_2 corresponding to each band was obtained by integration, the results being collected in Table 5. Calcined LDHs are known to possess basic sites of weak, medium and high strength, corresponding to respectively OH^- groups, Mg–O (or Li–O) ion pairs and surface O^{2-} ions [36]. The hydroxyl groups should function as Brønsted base sites, while the remaining sites can be expected to possess significant Lewis base character. From Table 5 it is apparent that calcined LiAl-3 possesses a greater abundance of all three site types compared to the calcined Mg–Al LDH, the predominant sites being of medium basicity, which likely correspond to Li^+–O^{2-} pairs. These results contrast with a recent report by Angelescu et al. [37] concerning the results of CO_2 TPD on calcined Mg–Al and Li–Al LDHs. The two materials were found to possess similar total basic site concentrations, although the calcined Mg–Al LDH possessed a higher concentration of strong basic sites. Again, differences in the calcination protocol applied may account for these contrasting results. Indeed, in the study by Angelescu et al., the calcined form of the Li–Al LDH presented a main phase corresponding to $LiAlO_2$, whereas the material in our study was X-ray amorphous.

At first sight, the Hammett indicator and CO_2 TPD measurements present apparently contrasting results. However, it should be appreciated that Hammett indicator measurements provide a measure of Brønsted basicity only, given that the H_- scale cannot be directly related to the strength of Lewis base sites. In the case of CO_2 TPD, a qualitative measure is provided of the strength of both Brønsted and Lewis base sites. Furthermore, while the Hammett indicator results suggest that the calcined Mg–Al LDH contains sites of higher Brønsted basicity than the calcined Li–Al LDH (in the presence of liquid methanol), the measurements provide no indication of basic site concentrations. (Attempts to obtain basic site strength distributions by means of benzoic acid titration in the presence of Hammett indicators gave poorly reproducible results, due to the difficulty in accurately determining end points.) The information provided by the two methods can therefore be considered complimentary, and it can be concluded that while the Mg–Al sample may contain sites of stronger Brønsted basicity than its Li–Al analog, the latter is indicated to possess higher total basicity.

Table 5
Results of CO_2 TPD measurements on calcined layered double hydroxides[a]

Sample	CO_2 desorbed (μmol g(cat)$^{-1}$)	Temperature range (°C)	Peak temperature (°C)
$Mg_{0.73}Al_{0.27}$			
First peak	21.9	93–184	145
Second peak	29.3	184–457	228
Third peak	7.3	457–500	500
Total	58.5		
LiAl-3			
First peak	24.5	81–190	143
Second peak	47.2	190–454	228
Third peak	9.7	454–500	500
Total	81.4		

[a] Calcination at 450 °C for 2 h.

3.2. Transesterification of glyceryl tributyrate with methanol

For the purposes of catalyst screening, samples were tested in a model reaction, namely the transesterification of glyceryl tributyrate with methanol to form methyl butanoate. Collected in Table 6 are the initial reaction rates and the percent methyl ester formed after 180 min for the different catalysts tested. Triglyceride transesterification consists of a sequence of three reversible reactions, in which the triglyceride is successively transformed into diglyceride, monoglyceride and finally glycerol and methyl ester (Scheme 1). Cantrell et al. [15] have reported that hydrotalcite-catalyzed methanolysis of glyceryl tributyrate proceeds without an induction period

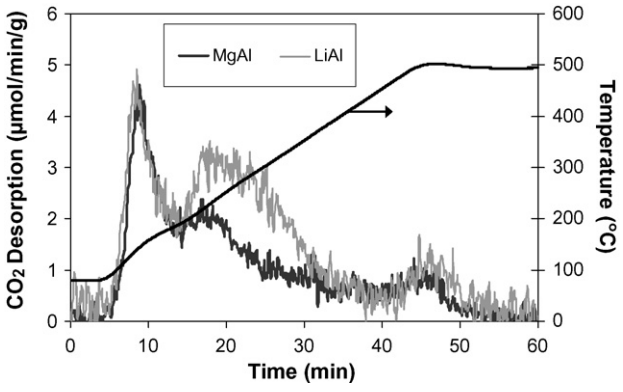

Fig. 6. TPD profiles of CO_2 adsorbed on calcined $Mg_{0.73}Al_{0.27}$ and LiAl-3.

Table 6
Transesterification of glyceryl tributyrate with methanol

Catalyst[a]	Yield of methyl butanoate after 180 min (%)	Initial rate (mol g(cat)$^{-1}$ h^{-1})	Surface area normalized rate ($\times 10^3$ mol g(cat)$^{-1}$ h^{-1} m^{-2})
Blank	0.3	–	–
$Mg_{0.73}Al_{0.27}$	32.0	0.27	1.29
$Mg_{0.66}Al_{0.34}$	19.7	0.22	0.91
$Mg_{0.69}Fe_{0.31}$	23.9	0.19	0.89
MgO	37.1	0.42	2.05
LiAl-1	>98	9.82	64.6
LiAl-2	>98	>10	>45.2
LiAl-3	>98	>10	>44.1

[a] Catalysts calcined at 450 °C for 2 h.

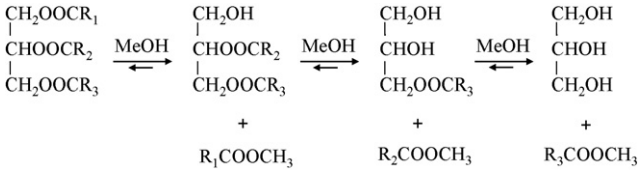

Scheme 1. Generalized scheme for triglyceride transesterification with methanol.

and with simultaneous formation of the methyl ester and diglyceride. The yield of these primary products initially increases linearly with triglyceride consumption, after which secondary transesterification of the diglyceride to monoglyceride occurs. Similar behavior was observed with the catalysts employed in this study. Fig. 7 shows a plot of the reactant and product concentrations for the calcined form of LiAl-1. The concentration of diglyceride initially increases but then rapidly falls off as the monoglyceride is formed, which in turn is consumed. Within the timeframe of the experiment (180 min), complete consumption of both the triglyceride and diglyceride was observed in the presence of the calcined Li–Al catalysts, although a small amount of monoglyceride remained; the latter is a consequence of the fact that transesterification is a reversible process, i.e., under the reaction conditions used the yield of methyl ester at equilibrium is less than 100%.

Due to the high activity of the Li–Al catalysts it was difficult in some cases to determine the initial rates for ester formation accurately, however, they are estimated to be in all cases close to, or in excess of, 10 mol g(cat)$^{-1}$ h^{-1}. In contrast, the calcined Mg–Al and Mg–Fe LDHs displayed rates in the range 0.19–0.27 mol g(cat)$^{-1}$ h^{-1}, while the sample of precipitated MgO was slightly more active (0.42 mol g(cat)$^{-1}$ h^{-1}). Consideration of the surface area normalized initial reaction rates for the calcined Mg–Al, Mg–Fe and MgO catalysts suggests that replacing Al with Fe does not significantly affect catalyst activity. Further, the calcined hydrotalcite with Mg/Mg + Al = 0.73 is more active than that with Mg/Mg + Al = 0.66. This is consistent with the results of Cantrell et al. [15], who found that the normalized rates for glyceryl tributyrate methanolysis increased with increasing Mg content (and intra-layer charge density) for a series of hydrotalcites

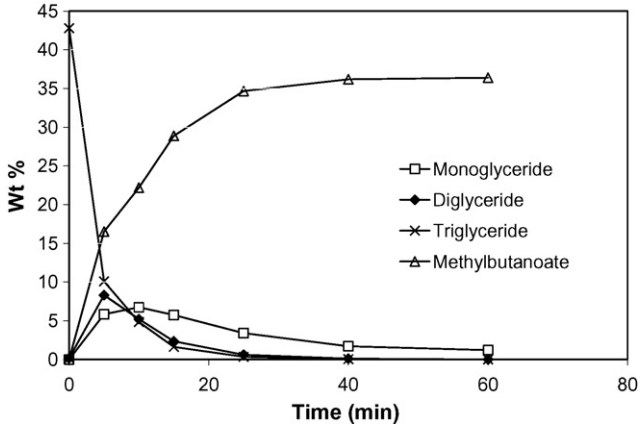

Fig. 7. Transesterification of glyceryl tributyrate with methanol catalyzed by LiAl-1 at 65 °C.

with Mg/Mg + Al in the range 0.45–0.75 which had been calcined and rehydrated. The increased intralayer electron density of Mg-rich hydrotalcites would be expected to correlate with an increase in basicity. Calcined hydrotalcites have also been used as catalysts in the methanolysis of soybean oil [14]. In that study, catalyst activity likewise increased with Mg content up to a maximum at Mg/Mg + Al = 0.75, after which it decreased. This trend correlated directly with the measured Brønsted basicity of the catalysts as determined by benzoic titration in the presence of Hammett indicators.

These results show the Li–Al catalysts to be far more active than the other LDH-derived catalysts tested. This finding correlates to some degree with the results of the CO_2 TPD measurements, showing higher concentrations of medium and strong base sites for calcined LiAl-3, although such a large difference in transesterification activity between the Li–Al and Mg–Al catalysts would not necessarily be predicted on the basis of the TPD results. Nevertheless, it follows that sites of medium and strong basicity are indicated to be the main sites active in transesterification catalyzed by the calcined Li–Al LDHs.

3.3. Transesterification of soybean oil with methanol

Soybean oil methanolysis was performed at reflux temperature, using a fixed methanol to soybean oil mole ratio of 15:1 and a catalyst charge of 1 wt.% (based on the quantity of soybean oil used). The results are collected in Table 7. Little variation was observed in the yield of methyl esters obtained with the three Li–Al catalysts, consistent with the results of the glyceryl tributyrate transesterification experiments. Likewise, the Li–Al catalysts were considerably more active than the MgO and calcined Mg–Al LDHs.

In a previous paper [21] we noted that the calcination temperature of $[LiAl_2(OH)_6](CO_3)_{0.5}\cdot nH_2O$ exerts a significant influence on its activity in soybean oil transesterification with methanol. A temperature of 400–450 °C was found to be optimal, corresponding to decomposition of the layered double hydroxide to an amorphous mixed oxide. In order to provide greater insight into the decomposition of $[LiAl_2(OH)_6](CO_3)_{0.5}\cdot nH_2O$, XRD measurements were carried out on LiAl-3 over the temperature range 20–700 °C using a heated sample stage. Additionally, BET surface area measurements were performed on samples of LiAl-3 calcined at different temperatures in this range. The resulting data are collected in Table 8 and Fig. 8. Table 8 also includes the results of soybean oil methanolysis reactions catalyzed by the calcined LiAl-3

Table 7
Transesterification of soybean oil with methanol

Catalyst[a]	Catalyst charge (wt.%)	Reaction time (h)	Yield of methyl esters (%)
LiAl-1	1	2	77.6
LiAl-2	1	2	79.0
LiAl-3	1	2	83.1
MgO	1	2	≤2
$Mg_{0.73}Al_{0.27}$	3	6	13.6

[a] Catalysts calcined at 450 °C for 2 h.

Table 8
Dependence of methyl esters yield and catalyst surface area on calcination temperature of LiAl-3[a]

Calcination temperature (°C)	Yield of methyl esters (%)	Catalyst surface area ($m^2\ g^{-1}$)
–	≤2	96
300	36.6	292
350	42.9	310
400	60.6	235
450	71.5	227
500	71.9	232
600	40.8	228
700	16.8	123

[a] Reaction conditions: 1 h reaction time, 1 wt.% catalyst, MeOH:oil = 15:1, reflux temperature.

samples. As shown in Fig. 8, collapse of the layered structure is already apparent after calcination at 200 °C for 2 h. Diffractograms obtained in the temperature range 200–500 °C are consistent with the amorphous nature of the mixed Li–Al oxide decomposition product, although broad, weak diffraction lines at ca. $2\theta = 37^\circ$ and 65° suggest the presence of poorly crystalline γ-Al_2O_3. At 600 °C new diffraction lines appear corresponding to $LiAlO_2$ (JCPDS file 044–0224), these lines becoming narrower and more intense upon heating to 700 °C.

Published thermogravimetric data [21,38] indicate that decomposition of $[Al_2Li(OH)_6](CO_3)_{0.5}{\cdot}nH_2O$ commences at 130 °C and extends up to ca. 450 °C, with a DTG maximum at 204 °C. Initial weight loss is believed to correspond to elimination of the interlayer water, however, it is clear that this process overlaps with carbonate decomposition and the elimination of hydroxyl groups. IR data suggest that CO_2 is eliminated in successive stages, with residual carbonate ions present at temperatures as high as 500 °C [38]. As shown in Table 8, calcination at 450–500 °C is optimal for the activity of the catalyst in soybean methanolysis. Based on the foregoing, this temperature range can be seen to represent an optimum for decomposition of the LDH to the amorphous mixed oxide, without formation of crystalline $LiAlO_2$. Although maximum surface area is developed at around 300–350 °C, thermogravimetric data indicate that at temperatures below 450 °C elimination of CO_2 and H_2O is incomplete, and hence the formation of the basic Li–O and lattice O^{2-} sites required for transesterification activity is similarly incomplete.

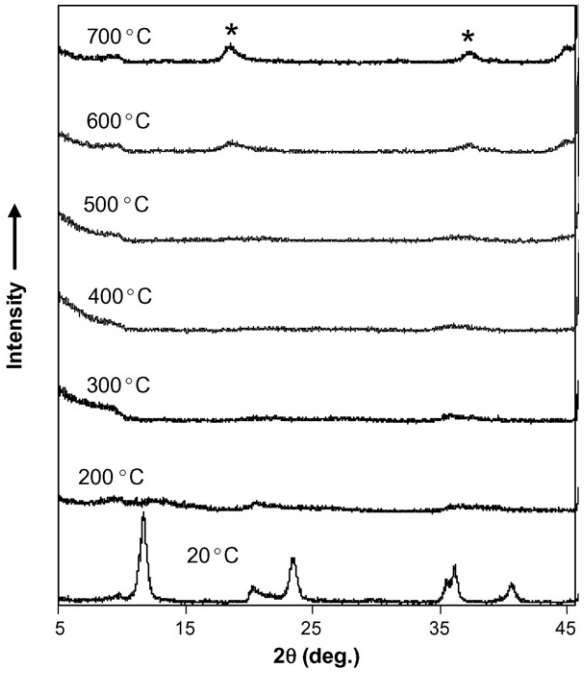

Fig. 8. *In situ* powder X-ray diffractograms of LiAl-3 after heating at temperatures in the range 200–700 °C. Diffractograms were recorded after a period of 2 h at the temperature indicated. *Diffraction line due to $LiAlO_2$.

Previously we have attempted to confirm the heterogeneous nature of a calcined $[LiAl_2(OH)_6](CO_3)_{0.5}{\cdot}nH_2O$ catalyst in soybean oil methanolysis by performing hot filtration and catalyst recycling experiments [21]. Results showed that the catalyst maintained a high level of activity over several cycles (when re-calcined between cycles), although analysis of the water-soluble extract from the reaction mixture indicated that a small amount of lithium was leached from the catalyst (equivalent to 3% of the total Li content). As a further test of whether the observed catalysis is truly heterogeneous, a sample of calcined LiAl-2 was stirred in methanol for 1 h, after which the catalyst was removed by filtration. Soybean oil was added to the filtrate and transesterification performed for 1 h under the standard conditions given in Section 2.4. Analysis of the reaction mixture revealed the presence of only a trace of methyl esters (<0.5% yield), suggesting that calcined $[LiAl_2(OH)_6](CO_3)_{0.5}{\cdot}nH_2O$ is indeed a heterogeneous transesterification catalyst.

In this context, analysis of the spent LiAl-1, LiAl-2 and LiAl-3 catalysts from the soybean oil methanolysis runs was of interest. As shown in Table 1, the Al/Li stoichiometries of the used catalysts measured by ICP-OES are close to the values measured for the uncalcined and calcined LDH samples, although in each case a slight increase in the stoichiometry is observed, suggestive of possible lithium loss. However, based on the experimental error of the analysis method (estimated at ±5% relative), none of the observed increases is statistically significant. In contrast, significant differences are observed in the absolute values of the Li and Al concentrations in the calcined and spent LiAl-1 and LiAl-3 catalysts, the lower Li and Al concentrations in the spent catalysts reflecting their higher oxygen and carbon contents (see below).

XPS data for the Li–Al LDH samples, both before and after calcination, as well as after use in soybean oil transesterification, are collected in Table 1. The observed Li 1s binding energies proved to be of little diagnostic value, the uncalcined, calcined and spent catalyst samples in each case showing a weak feature at 55.2 ± 0.2 eV. Binding energy data for Li are sparse due to the poor response of Li in XPS (the atomic sensitivity factor being 0.02 relative to F 1s = 1.00 [39]), although the value of 55.2 eV is close to values of 54.9 eV and 55.3 eV which have been reported for LiOH and Li_2CO_3, respectively [40]. O 1s XPS lines for the various Li–Al samples were generally symmetric and not readily deconvoluted into constituent states. However, a shift in the position of the O 1s

signal from 531.7 eV for the uncalcined LDHs to 530.6 ± 0.3 eV for the calcined materials is consistent with their increased oxidic character [15,41,42]. Analysis of the carbon 1s spectra confirmed the presence of a Li_2CO_3-type environment in the uncalcined LDHs, a signal observed at 289.1 eV being close to values reported for Li_2CO_3 [42,43]. Upon calcination, the intensity of this signal was greatly reduced, consistent with conversion of the LDH to the mixed oxide, although it failed to disappear completely. The same signal was also exhibited by the spent catalysts, although its intensity was not reproducibly greater than that in the freshly calcined samples. However, given that the calcined samples were briefly exposed to air during XPS sample preparation, we cannot rule out that this may have influenced the observed surface carbonate concentration. Also of note is the observation of high carbon concentrations measured by XPS in the spent Li–Al catalysts, typically around 15 at.%. This contrasts with carbon concentrations of ∼7 at.% measured for the freshly calcined samples, and suggests the presence of residual organic species that were not removed by washing.

The atomic Al/Li ratios derived from the XPS data are also collected in Table 1. Values for the uncalcined LDHs were consistently higher than the expected stoichiometric value of 2, indicative of surface enrichment by Al. Upon calcination the Al/Li ratio decreased to the expected value, suggesting that some degree of surface reorganization occurs during calcination, with the final surface corresponding to the Li–Al mixed oxide. Conversion of $[LiAl_2(OH)_6](CO_3)_{0.5}{\cdot}nH_2O$ to the mixed oxide, a process that involves dehydration and carbonate decomposition, is also reflected in the observed increases in Li and Al atomic concentrations and concomitant decreases in O and C concentrations. Measured Li atomic concentrations for the calcined samples, while similar, followed the order LiAl-3 > LiAl-2 > LiAl-1. This is the same ordering observed for catalyst activity in soybean oil methanolysis (Table 7), suggesting a direct correlation between catalyst activity and surface Li content.

For the spent catalysts, the Li and Al atomic concentrations fall between those of the uncalcined and calcined LDH, as do the O and C values. While the increased C concentration reflects the presence of residual organic species, the increased O concentration is consistent with partial rehydration of the surface and possible CO_2 adsorption (processes which may have occurred during catalyst use or the subsequent work-up). The Al/Li ratios for the spent catalysts also fall between values observed for the uncalcined and calcined LDH samples. While this increase in Al/Li ratio upon catalyst use may be a consequence of Li leaching from the catalyst surface, as indicated above, typically only 3% of the catalyst Li content was leached during use. As shown in Table 2, average crystallite sizes in the 0 0 *l* direction spanned the range 11–26 nm; assuming a mean XPS analysis depth of 5 nm, it follows that a significant fraction of the Li in the samples should be analyzed and hence that this degree of leaching from the surface should have relatively little effect on the observed Li atomic concentration. Rather, the observed increases in the Al/Li ratio and O atomic concentration appear to reflect a partial reversion of the surface to an LDH-like phase, albeit that the bulk sample remained amorphous according to XRD data. Consistent with this idea, attempts to recycle the used catalysts in soybean oil methanolysis without first re-calcining them afforded low yields of methyl esters, although the presence of residual organic compounds may contribute to the decreased catalyst activity. In a typical experiment, for example, a methyl ester yield of 10% was measured after 1 h reaction time for recycled LiAl-1, versus a yield of 58% for recycled catalyst which was first re-calcined at 450 °C.

4. Conclusions

The results from this study confirm our earlier findings that calcined $[Al_2Li(OH)_6](CO_3)_{0.5}{\cdot}nH_2O$ is a highly effective catalyst for the transesterification of soybean oil with methanol. The three different co-precipitation procedures examined for $[Al_2Li(OH)_6](CO_3)_{0.5}{\cdot}nH_2O$ preparation were found to afford the LDH as a pure phase according to powder X-ray diffraction, although differences were observed in the crystallinity and morphology of the LDH. The calcined samples were found to show similar catalytic properties in the methanolysis of glyceryl tributyrate and soybean oil, being considerably more active than calcined Mg–Al and Mg–Fe LDHs. XPS and XRD data indicate that an amorphous Li–Al mixed oxide is the catalytically active phase. Elemental analysis data collected on the used catalysts indicate that lithium leaching from calcined $[LiAl_2(OH)_6](CO_3)_{0.5}{\cdot}nH_2O$ is minimal during short duration batch transesterification experiments. This finding is consistent with the results of analyses for Li performed on the filtrate from soybean transesterification experiments. However, these results say little about the stability of the catalyst under likely industrial operating conditions. More specifically, it is unlikely that even a relatively low rate of lithium leaching from the catalyst can be tolerated when the catalyst is applied in fixed bed mode (when there is little chance for leached lithium to re-adsorb on the catalyst) and the catalyst is operated for periods of hundreds and possibly thousands of hours. For this reason, fixed bed experiments are currently in progress to address this issue.

Acknowledgements

The authors thank Gerald Thomas for performing the XRD and ICP-OES measurements. The Commonwealth of Kentucky (Governor's Office of Energy Policy) is thanked for financial support.

References

[1] F. Ma, M.A. Hanna, Bioresour. Technol. 70 (1999) 1.
[2] U. Meyer, W.F. Hoelderich, Appl. Catal. A 178 (1999) 159.
[3] A. Corma, S. Iborra, S. Miquel, J. Primo, J. Catal. 173 (1998) 315.
[4] A. Radich, www.eia.doe.gov/oiaf/analysispaper/biodiesel/.
[5] G.R. Peterson, W.P. Scarrah, J. Am. Oil Chem. Soc. 61 (1984) 1593.
[6] S. Gryglewicz, Bioresour. Technol. 70 (1999) 249.
[7] E. Leclercq, A. Finiels, C. Moreau, J. Am. Oil Chem. Soc. 78 (2001) 1161.

[8] M. López Granados, M.D. Zafra Poves, D. Martín Alonso, R. Mariscal, F. Cabello Galisteo, R. Moreno-Tost, J. Santamaría, J.L.G. Fierro, Appl. Catal. B 73 (2007) 317.
[9] X. Liu, H. He, Y. Wang, S. Zhu, Catal. Commun. 8 (2007) 1107.
[10] W. Xie, H. Peng, L. Chen, Appl. Catal. A 300 (2006) 67.
[11] W. Xie, H. Li, J. Mol. Catal. A 255 (2006) 1.
[12] W. Xie, X. Huang, Catal. Lett. 107 (2006) 53.
[13] R.S. Watkins, A.F. Lee, K. Wilson, Green Chem. 6 (2004) 335.
[14] W. Xie, H. Peng, L. Chen, J. Mol. Catal. A 246 (2006) 24.
[15] D.G. Cantrell, L.J. Gillie, A.F. Lee, K. Wilson, Appl. Catal. A 287 (2005) 183.
[16] R. Sercheli, R.M. Vargas, U. Schuchardt, J. Am. Oil Chem. Soc. 76 (1999) 1207.
[17] L. Bournay, D. Casanave, B. Delfort, G. Hillion, J.A. Chodorge, Catal. Today 106 (2005) 190.
[18] G. Hillion, S. Leporq, D. Le Pennec, B. Delfort, European Patent EP1468734 (2004); G. Hillion, S. Leporq, D. Le Pennec, B. Delfort, U.S. Patent Application 0234448 (2004).
[19] A. Corma, S.B.A. Hamid, S. Iborra, A. Velty, J. Catal. 234 (2005) 340.
[20] M.B.J. Roeffaers, B.F. Sels, H. Uji-i, F.C. De Schryver, P.A. Jacobs, D.E. De Vos, J. Hofkens, Nature 439 (2006) 572.
[21] J.L. Shumaker, C. Crofcheck, S.A. Tackett, E. Santillan-Jimenez, M. Crocker, Catal. Lett. 115 (2007) 56.
[22] W.T. Reichle, J. Catal. 94 (1985) 547.
[23] E. Chenu, G. Jacobs, A.C. Crawford, R.A. Keogh, P.M. Patterson, D.E. Sparks, B.H. Davis, Appl. Catal. B 59 (2005) 45.
[24] C.J. Serna, J.L. Reddon, J.E. Iglesias, Clays Clay Miner. 30 (1982) 180.
[25] I. Sissoko, E.T. Iyagba, R. Sahai, P. Biloen, J. Solid State Chem. 60 (1985) 283.
[26] M.A. Ulibarri, M.J. Hernandez, J. Cornejo, C.J. Serna, Mater. Chem. Phys. 14 (1986) 569.
[27] S. Krumm, Winfit. Available at: www.xray.cz/ecm-cd/soft/xray/index0114.html.
[28] K. Tanabe, M. Misono, Y. Ono, H. Hattori, Stud. Surf. Sci. Catal. 51 (1989) 1.
[29] G. Gelbard, O. Bres, R.M. Vargas, F. Vielfaure, U.F. Schuchardt, J. Am. Oil Chem. Soc. 72 (1995) 1239.
[30] W.T. Reichle, S.Y. Kang, D.S. Everhardt, J. Catal. 101 (1986) 352.
[31] F. Rey, V. Fornes, J.M. Rojo, Faraday Trans. 88 (1992) 2233.
[32] P. Kuśtrowski, A. Wigrzyn, A. Rafalska-Lasocha, A. Pattek-Janczyk, R. Dziembaj, Clays Clay Miner. 53 (2005) 18.
[33] K.S.W. Sing, D.H. Everett, R.A.W. Haul, L. Moscou, R.A. Pierotti, J. Rouquerol, T. Siemieniewska, Pure Appl. Chem. 57 (1985) 603.
[34] V. Rives, in: V. Rives (Ed.), Layered Double Hydroxides: Present and Future, Nova Science Publishers, New York, 2001 (Chapter 8 and references therein).
[35] W. Kagunya, Z. Hassan, W. Jones, Inorg. Chem. 35 (1996) 5970.
[36] J.I. Di Cosimo, V.K. Diez, M. Xu, E. Iglesia, C.R. Apesteguia, J. Catal. 178 (1998) 499.
[37] E. Angelescu, O.D. Pavel, R. Bîrjega, R. Zăvioanu, G. Costentin, M. Che, Appl. Catal. A: Gen. 308 (2006) 13.
[38] M.J. Hernandez, M.A. Ulibarri, J. Cornejo, M.J. Pena, C.J. Serna, Thermochim. Acta 94 (1985) 257.
[39] C.D. Wagner, L.E. Davis, M.V. Zeller, J.A. Taylor, R.M. Raymond, L.H. Gale, Surf. Interf. Anal. 3 (1981) 211.
[40] Handbook of the Elements and Native Oxides, XPS International Inc. Available at: http://www.xpsdata.com/XI_BE_Lookup_table.pdf.
[41] X.D. Peng, D.A. Richards, P.C. Stair, J. Catal. 121 (1990) 99.
[42] J.R. Hoenigman, R.G. Kiel, in: R.O. Bach (Ed.), Lithium: Curr. Appl. Sci., Med. Technol., Wiley, NY, 1985, pp. 233–255.
[43] J.P. Contour, A. Salesse, M. Froment, M. Garreau, J. Thevenin, D. Warin, J. Microsc. Spectrosc. Electron. 4 (1979) 483.